Journal Pre-proofs

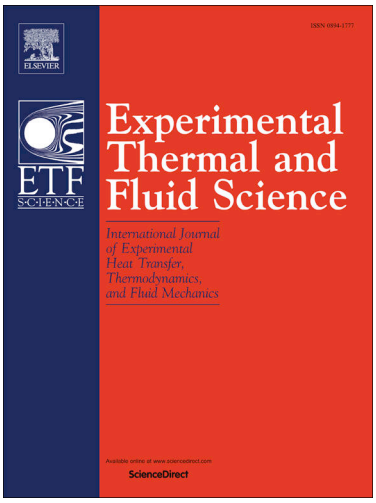

Experimental Study of Horizontally Lifted High-speed Nonpremixed Flame Jets

Q. Wang, P. Zhu, X.H. Mei, V. Foroughi, J. Casal, E. Planas, A. Albadi, Y.C. Zhang, Y. Zhang

PII: S0894-1777(22)00170-4
DOI: https://doi.org/10.1016/j.expthermflusci.2022.110774
Reference: ETF 110774

To appear in: *Experimental Thermal and Fluid Science*

Received Date: 18 February 2022
Revised Date: 18 August 2022
Accepted Date: 4 September 2022

Please cite this article as: Q. Wang, P. Zhu, X.H. Mei, V. Foroughi, J. Casal, E. Planas, A. Albadi, Y.C. Zhang, Y. Zhang, Experimental Study of Horizontally Lifted High-speed Nonpremixed Flame Jets, *Experimental Thermal and Fluid Science* (2022), doi: https://doi.org/10.1016/j.expthermflusci.2022.110774

Experimental Study of Horizontally Lifted High-speed Nonpremixed Flame Jets

Q. Wang[a*], P. Zhu[a], X.H. Mei[a], V. Foroughi[b], J. Casal[b], E. Planas[b], A. Albadi[c], Y.C. Zhang[c], Y. Zhang[c*]

[a] *School of Mechanical Engineering, Shanghai Jiao Tong University, Shanghai 200240, China*

[b] *Centre for Technological Risk Studies (CERTEC), Universitat Politècnica de Catalunya·BarcelonaTech, Av. Eduard Maristany, 16, 08019-Barcelona, Spain*

[c] *Department of Mechanical Engineering, University of Sheffield, Mappin Street, Sheffield, S1 3JD, UK*

[*]Corresponding author: qianwang@sjtu.edu.cn; yz100@sheffield.ac.uk

Abstract

This paper presents an experimental study on horizontally jet flames with rather high velocities (58 m/s-167 m/s, Reynolds number up to 3.0×10^5), which mainly fall in the momentum-controlled region. Both high-speed schlieren and color imaging techniques have been adopted to obtain the time-resolved images, based on which the flame and flow dynamics has been discussed comprehensively. Under the test conditions, all the flames have shown lift-off characteristics. The dynamic mode decomposition (DMD) and proper orthogonal decomposition (POD) analysis has been performed to reveal the flame and flow fluctuating frequency and the corresponding spatial distribution. The results have shown two high frequency modes at 269 Hz and 537 Hz in the lifted-off jet region, which may come from the test bench vibration. The statistics of flame length, height and lift-off distance have been presented, which have been compared with previously reported data at lower velocities. The comparison indicates that the flame behaviors have shown quite dramatic differences in the buoyancy and momentum-controlled regions. The present experiments have extended the research of horizontally placed jet flames to a wider velocity range, which has greatly broadened our knowledge of the lift-off jet flame behaviors under high velocity conditions.

Keywords：horizontal jet flame; lift-off distance; flame length; flame height; dynamic mode decomposition.

1. Introduction

Non-premixed turbulent jet flames are widely adopted for industrial burners and exist in many occasions of fire hazards, such as fuel leakage from pressurized tankers and pipelines. A non-premixed jet flame has a tendency to lift off from the burner nozzle position when the jet velocity of the flame is over a critical value [1-3]. With the increasing of the jet velocity, the lifted height will increase and the flame may be blown off abruptly after a certain height [4]. The lift-off flame instability originates from its anchoring in an unstable turbulent jet flow, which has attracted intensive attentions from researchers in combustion community [5-7]. Efforts have been devoted to explore the most relevant parameters, including fuel type [8-10], nozzle exit dimension [11, 12], jet velocity [11-15], pressure [16-18], etc. Wohl et al. [19] proposed that the lift-off phenomena would occur when the combustion velocity and the flow velocity of local gas at the maximum laminar flame speed were equal. Gollahalli [20] argued that the flame anchoring position features a balance between the local flow velocity and the normal flame propagation velocity. Demore et al. [21] employed high-speed laser tomography to visualize the vortices generated in a non-premixed lifted flame in the hysteresis zone. It is shown that the appearances of lobe-like flames are due to the streamwise counter-rotating vortices. The lift-off height has been studied as an important parameter closely related with the flame instability phenomena [8, 16, 22]. Experimental investigations found that for a given gas, the flame lift-off height varies linearly with the jet exit velocity, which is independent of the burner diameter in most cases [11]. However, deviations from the linear increasing trend have been reported in coflow jet experiments by Brown et al. [23] and Guiberti et al. [24]. Erete et al. [25] reported that for non-premixed CH_4 air flames, the flame lift-off height increased with the increase percentage of CO_2 dilution. Hu et al. [26] conducted comparative experiments on turbulent jet diffusion propane flames at different ambient pressures.

The results indicate that at a reduced ambient pressure of 64 kPa, the lift-off velocities are lower, while the lift-off heights are increased.

Great efforts have been made to establish suitable correlations between lift-off height and the relevant parameters. Based on the observation that for a free jet diffusion flame, the lift-off height is independent of the nozzle diameter, simple linear correlations of lift-off height and jet exit velocity have been proposed in several literatures [27-29]. However, the results demonstrated that the lift-off height was greatly affected by the nozzle diameter in confined jets [28]. Hu et al. [29] established two sets of linear interpretations to correlate the lift-off height and fuel flow velocity at both normal and reduced ambient pressures. One set uses the original lift-off height, while the other incorporates the ratio between lift-off height and the nozzle diameter. The two sets of fitting curves both indicate that the lift-off height is much higher in the reduced pressure condition. Kalghatgi [11] proposed two non-dimensional groupings to establish the relationship, which was able to collapse onto a single curve for several different fuels at normal ambient pressure. One parameter is a Reynolds number based on laminar burning velocity S_L and the lift-off length L normalized by laminar flame thickness. The other parameter involves the fuel flow mean velocity at the exit normalized by S_L, which is multiplied with the density ratio between fuel and air. Bradley et al. [6] has derived a new dimensionless flow number by involving the S_L normalized jet velocity, a power function of Reynolds number as well as the pressure ratio between fuel and air. The lift-off height is normalized by nozzle diameter, while the fuel to air mole ratio leading to the maximum laminar burning velocity is introduced as a correction factor to deal with different fuel compositions. The modified relationship is able to correlate the lift-off height for a wide range of flow velocities and fuel types. It also improves the suitability for different ambient pressures.

Although extensive investigations have been conducted on the vertical lifted diffusion flames, only a few have focused on the horizontal jet flames. Different from vertical jets, the buoyancy force and initial momentum are not in the same line, which are divergent with an angle which can reach up to 90°. Comparative studies have been

conducted by changing the jet angle from 0° to 90° [30, 31]. Lowesmith and Hankinson [32] conducted large scale measurements for the horizontal natural gas with and without hydrogen enrichments. The flame length and the incident radiation were measured and analyzed comprehensively. Full scale tests have been conducted on horizontally oriented liquefied natural gas (LNG) jet fires [33]. A lifted height was observed, which contained unburnt fuel and air mixtures surrounded by blue premixed flames. The jet fires have shown being tilted upwards, which is quite different for the vertical jet flames. Different correlations have been proposed using global parameters to correlate the horizontal jet diffusion flame trajectory [34-36]. Recently, Liu et al. [37] established an improved model, which took the local buoyancy force and initial horizontal momentum into consideration. Zhou et al. [38] investigated the effect of jet exit geometry shape on the horizontal jet fires systematically, including circular, rectangular, equilateral triangle and elliptic exits. The tests focused on the transition regime from buoyancy to momentum-controlled flames. The results indicate that the exit shape plays an important role for air entrainment, which should be included in the correlations. The experimental data obtained by Smith et al. [39] indicated that the influence of burner geometry or its orientation was negligible when the Reynolds number is up to 12,500.

It is noticed that the experimental data of horizontal jet flames are still quite limited, especially for high Reynolds number conditions. In the current study, the test conditions have been extended to a wider range. The flame and flow field characteristics have been investigated comprehensively through time-resolved color and schlieren images respectively.

2. Experimental method

2.1 Experimental setup

The components of the flame jet setup have been shown in Fig.1(a), which include a propane cylinder, a valve, a pressure regulator, a flow meter, and nozzles of different sizes. Different jet conditions were obtained using a pressure regulator and three nozzles with diameters of 4 mm, 6 mm and 8 mm [40].

In the present study, in order to avoid the disturbance from the long jet flames, a modified schlieren setup is used, which has been shown in Fig.1(b). The setup consists of a point light source, two spherical concave mirrors, a knife edge, and a high speed camera. Different from the conventional Z-type setup, the light source and the camera are placed at the same side of the two mirrors. In this setup, the flame front will not affect the imaging components, while the test area can be changed simply by moving the mirrors and adjusting the light source and camera. Additional details of the schlieren imaging system and flame jet are shown in Table 1. Besides of the schlieren imaging, a phone camera was used to take the color flame images at a framing rate of 240 fps, with a resolution at 1280×720 pixels.

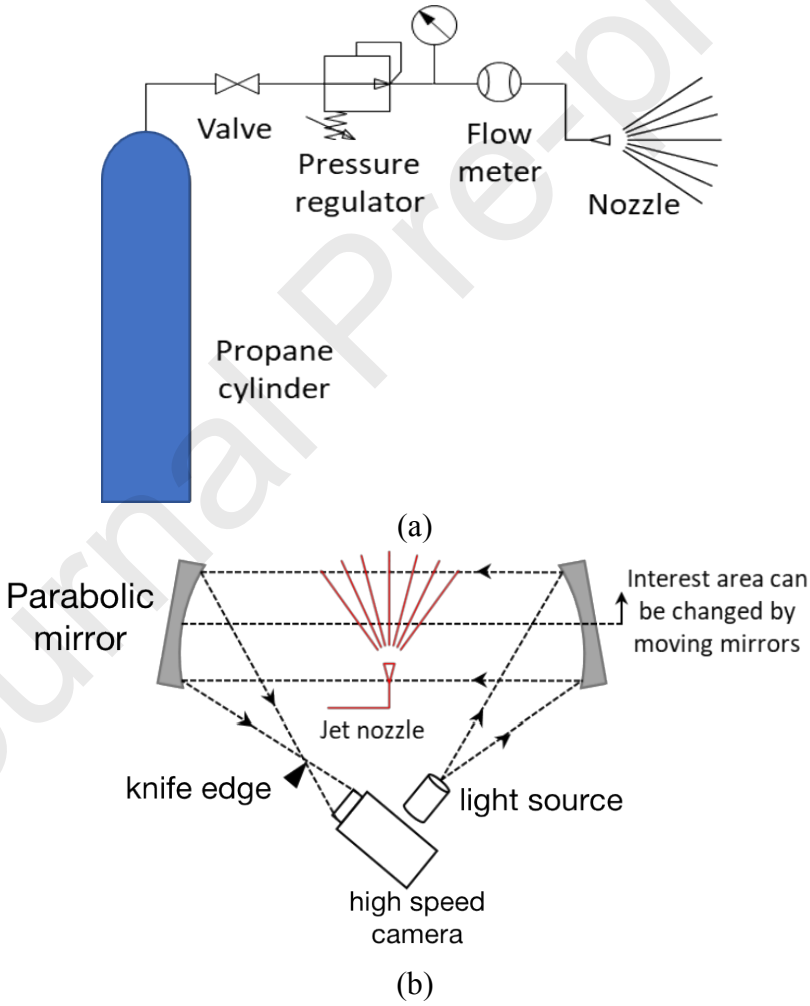

Fig.1 Experimental setups of (a) the jet flame, and (b) the schlieren imaging system.

Table 1 Details of the schlieren imaging system and flame jet conditions

Parameter	Value
Camera	Photron FASTCAM SA4
Lens	Nikkor Zoom MF 35-200mm f/3.5-4.5
Mirror size	30 [cm]
Shutter speed	1/333000 [1/s]
FPS	5000
Jet nozzle diameter	4,6,8 [mm]
Average mass flow rate	0.002- 0.012 [kg/s]
Absolute pressure	1.1-1.8 [bar]

2.2 Test conditions

The test conditions have been summarized in Table 2. The tests were conducted with three different jet nozzle diameters (d): 4 mm, 6 mm and 8 mm. In the present study, the Reynolds number and Froude number is calculated by $\mathrm{Re} = \frac{4\dot{m}}{\pi d \mu}$ and $Fr = \sqrt{u_e^2 / gd}$, where $\dot{m}$ is the mass flow rate, d is the nozzle diameter, μ is the dynamic viscosity of the fuel, u_e is the average jet velocity and g is the gravitational constant. The exit velocity (u_e) is changed in a range of 58 m/s to 167 m/s; the corresponding Reynolds number is from 52,000 to 300,000. The Froude number covers from 0.9×10^5 to 3.5×10^5, which is mainly belonging to the momentum-controlled regime ($Fr>1\times10^5$).

Table 2 Summary of experimental conditions

Case No.	d (mm)	u_e (m/s)	Re	Fr
1-8	4	58-88	5.2×10^4-7.8×10^4	0.9×10^5-2.0×10^5
9-19	6	90-148	1.2×10^5-2.0×10^5	1.4×10^5-3.7×10^5
20-22	8	131-167	2.3×10^5-3.0×10^5	2.2×10^5-3.5×10^5

2.3 Brief description of dynamic mode decomposition

The high speed schlieren imaging has supplied time-resolved information, which enables the application of dynamical analysis tools, such as proper orthogonal

decomposition method (POD) and dynamic mode decomposition (DMD). POD decomposes the original data into spatial multi-order modes (called eigenmodes) and corresponding time evolution coefficients of orthogonal modes. The order of the modes is from highest to lowest by the amount of energy it captures, given by the eigenvalues. The spectrum map of POD of each mode may be the result of multiple frequencies superimposed. Dynamic mode decomposition (DMD) is a data analysis method firstly proposed by Schmid [41, 42], aiming to better understand the coherent structures in a flow field. The DMD method treats the field change as a combination of linear dynamic processes, which can resolve the main frequency modes of the unsteady flow field as well as the spatial energy distribution at a certain frequency. Comparing with POD method, the single frequency characteristic of DMD mode is more convenient for researchers to analyze the flow mechanism. The recent application of DMD method to high speed planar laser-induced fluorescence, color and schlieren images have revealed the coherent structures of different frequencies up to 2400 Hz successfully [43-45]. In the present study, the DMD and POD analysis was conducted on schlieren images of three selected cases, following the procedure described below. The DMD analysis follows a similar strategy as in Ref. [45]. The main procedure is described below.

With a certain spatial-temporal data set $U = (u_1, u_2, ..., u_n)$, two subsets U_1 and U_2 are defined as:

$$U_1 = (u_1, u_2, ..., u_{n-1}) \tag{1}$$

$$U_2 = (u_2, u_3, ..., u_n) \tag{2}$$

The subscripts (1,2... n) represent the flow field at different time. Introducing the linear assumption between the neighboring moments, we may get that

$$U_2 = AU_1. \tag{3}$$

The features of matrix A is resolved by singular value decomposition, using the following equations.

$$U_1 = LSR^* \tag{4}$$

$$AU_1 = ALSR^* \Rightarrow AL = AU_1RS^{-1} \tag{5}$$

$$AL = U_2RS^{-1} \tag{6}$$

The similarity matrix A can be obtained by:

$$\tilde{A} = L^*AL = L^*U_2RS^{-1} \tag{7}$$

$$\tilde{A}\lambda_i = \xi_i\lambda_i \tag{8}$$

$$\varphi_i = L\xi_i \tag{9}$$

The eigenvalues involve imaginary and real parts, while the former represents the frequency and the latter indicates the growth rate corresponding to that specific mode.

$$\mathrm{f}_i = imag\frac{\ln\lambda_i}{2\pi\triangle t} \tag{10}$$

$$Rate = \mathrm{Re}\frac{\ln\lambda_i}{\triangle t} \tag{11}$$

Then, the flow field can be expressed as a superposition of different modes [46], which can be written as:

$$U_1 = (u_1, u_2, ..., u_{n-1}) = [\varphi_1, \varphi_2, ..., \varphi_r]\begin{bmatrix}\alpha_1 & & & \\ & \alpha_2 & & \\ & & \ddots & \\ & & & \alpha_3\end{bmatrix}\begin{bmatrix}1 & \lambda_1 & \cdots & \lambda_1^{n-1}\\ 1 & \lambda_2 & \cdots & \lambda_2^{n-1}\\ \vdots & \vdots & \vdots & \vdots\\ 1 & \lambda_r & \cdots & \lambda_r^{n-1}\end{bmatrix} = \mathrm{f}D \tag{12}$$

In Eq.(12), the matrix D contains the information of mode energy, while the row represents the mode energy variation over time and the column denotes the energy of different modes. The energy discussed in the present study follows Eq.(13), which is defined as the arithmetic square root of the amplitudes of a certain frequency at each time instant.

$$E_i = \sqrt{\sum_{k=1}^{n} (\varphi_i \alpha_i \lambda_i^{k-1})^2} = \varphi_i \alpha_i \sqrt{1^2 + (\lambda_i)^2 + \ldots (\lambda_i^{n-1})^2} \quad (13)$$

For the POD analysis, the diagonal matrix S in equation (4) consists of the square-root-values of the eigenvalues, whereas the matrix L consists of the spatial POD modes.

3. Results and discussion

3.1 Analysis of flame and flow dynamics

The flame color and schlieren snapshots of the selected cases are shown in Figs. 2 and 3. As shown in Fig.2, the lift-off phenomena can be observed clearly through the schlieren images. There are two regions in the left two images: the turbulent jet region with finer structures and the flame region with expansion and large structures. For the third case with the highest Reynolds number, the jet region is too long that the flame is out of the view region of the schlieren system. The corresponding color flame images shown in Fig.3 also show the lift-off distance between the nozzle exit and the flame base. The flame shows blue near the base region, which indicates the partially premixed combustion phenomena occurring in this area. In the downstream region, the flame shows to be yellow and reddish, which is due to the radiation of soot particles in the non-premixed combustion region.

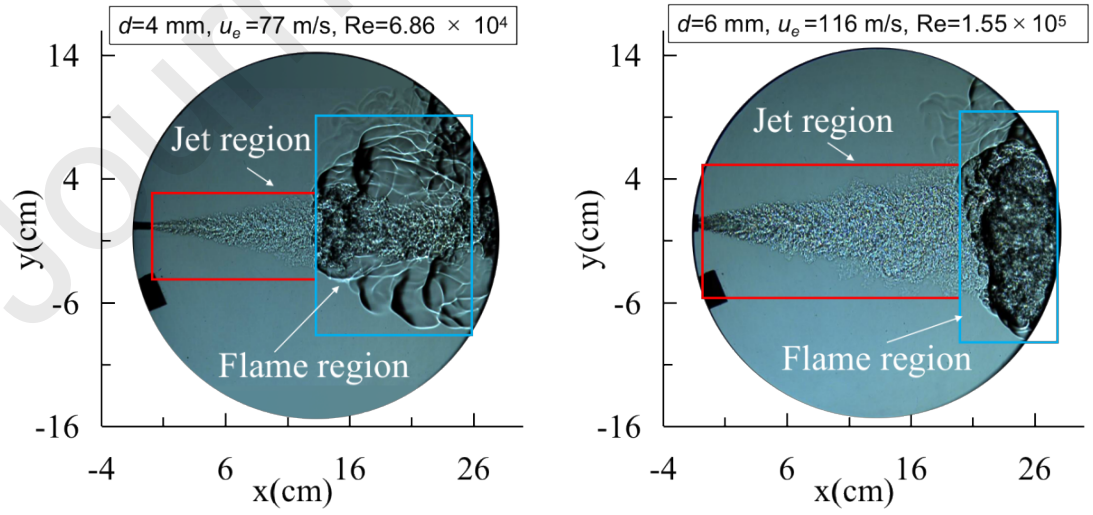

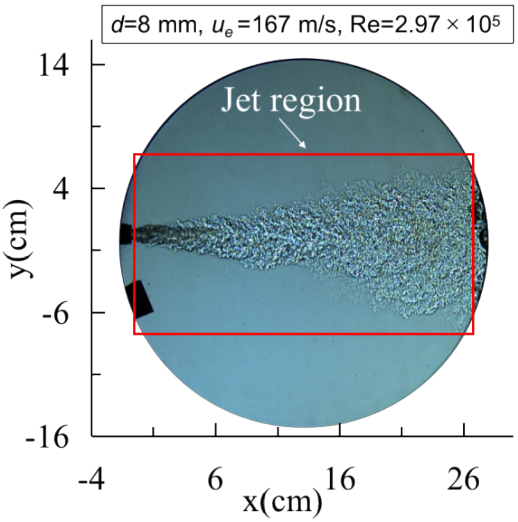

(c)

Fig 2. Schlieren images of the lift-off region and part of the flame region of three selected cases. (a) Test No.2; (b) Test No.9; (c) Test No.20.

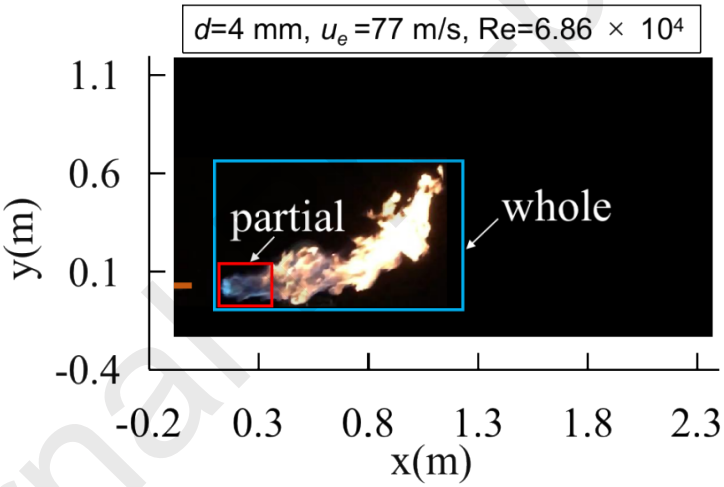

(a)

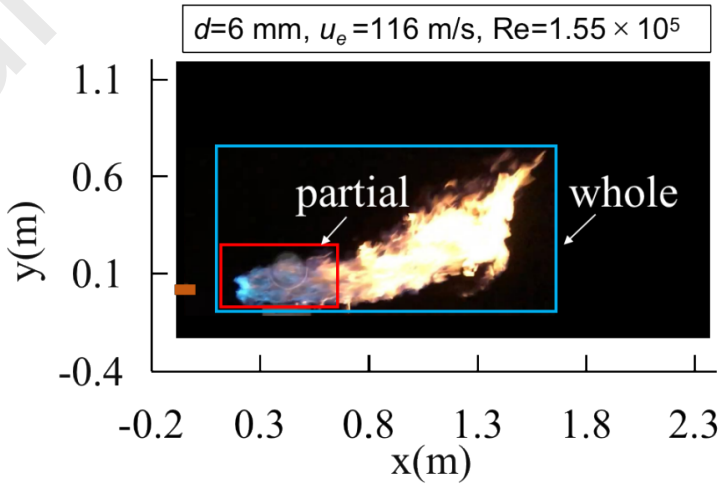

(b)

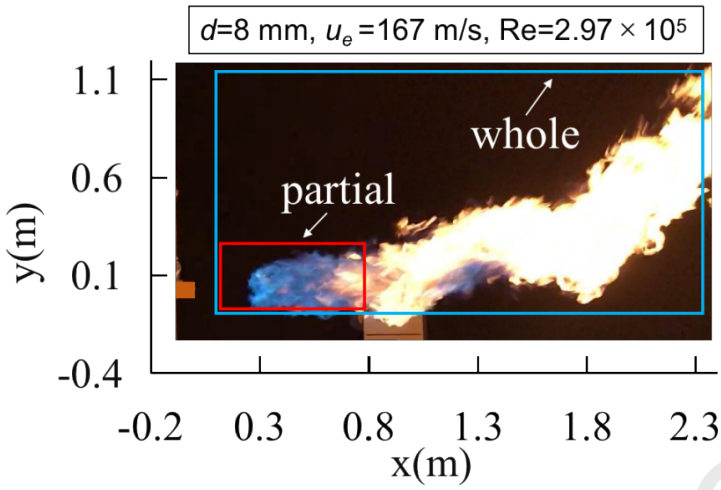

(c)

Fig 3. Color flame images of three selected cases
(a) Test No.2; (b) Test No.9; (c) Test No.20.

The DMD analysis has been conducted on the lift-off jet region of the selected cases. The frequency spectra and energy distributions at certain frequencies obtained from schlieren images have been presented in Figs.4-5. In Fig.4 (a), the real and virtual parts of the eigenvalues are shown. It can be seen that basically all the eigenvalues corresponding to the modes are distributed on or near the unit circle, indicating that these flame modes are neutral and stable in time. In each case, a total number of 1024 images are used and all cases have shown good convergence characteristics. It should be pointed out that similar distributions are also observed for the other DMD analysis results in the present study.

As shown in Fig.4(b-d), the spectra have involved a continuous distribution of frequencies from 0 to 1000 Hz, while the amplitude is decreasing with the increasing of frequencies. There are two peaks in all the three cases, at 269 Hz and its subharmonic of 537 Hz. One sample of the energy distribution at the two frequencies have been shown in Fig.5. It can be seen that the energy is distributed randomly with fine scale structures in the whole flow field. No obvious coherent structures can be observed. Besides, the POD analysis is also conducted on the schlieren images, while the spectral and spatial energy distribution of the first dominant mode has been shown in Fig.6. It can be seen that the first mode has involved the two frequency peaks of 269 Hz and 537 Hz for all the three cases. It is noticed that there are no dominant frequency peaks shown

on the spectra for higher POD modes. The spatial energy distribution has a similar pattern with the DMD results, while no obvious coherent structure can be observed. Both DMD and POD analysis has indicated that the two peaks are independent of the nozzle diameter and Reynolds number, which may come from a certain disturbance from the test bench.

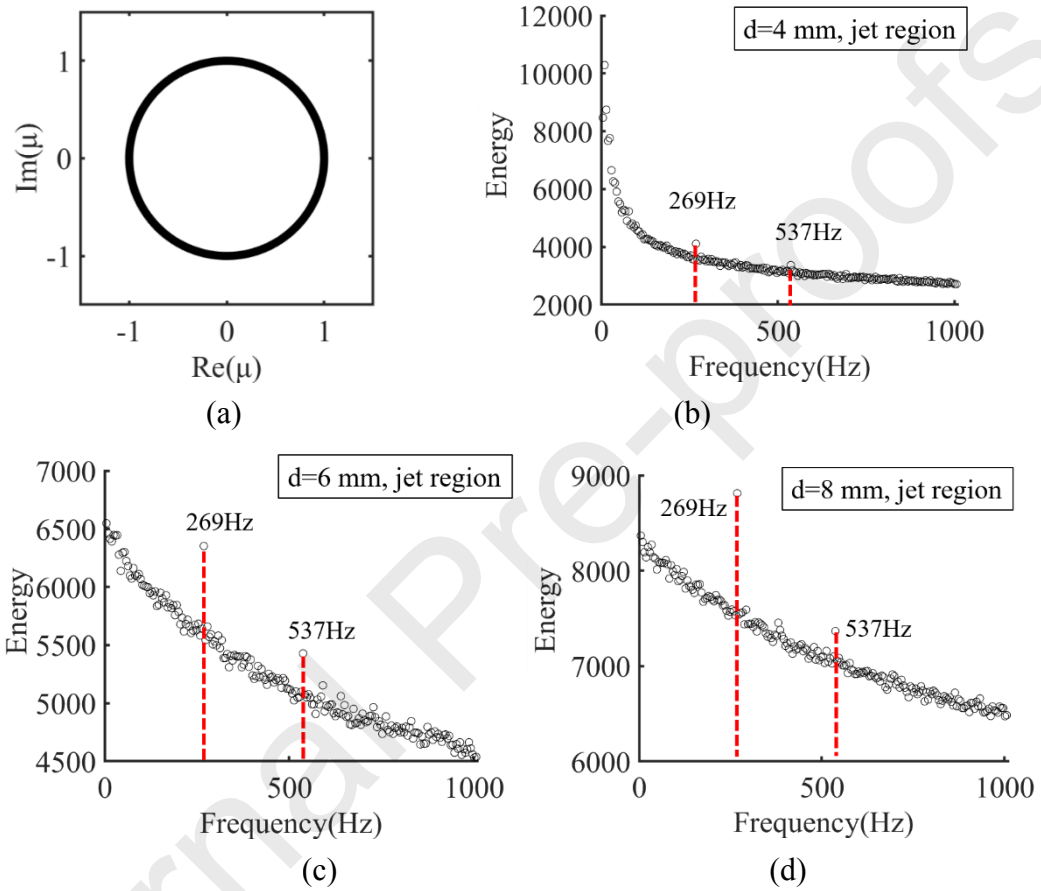

Fig.4 (a) DMD mode convergence and frequency spectra obtained from schlieren images for (b) Test No.2, (c) Test No.9, (d) Test No.20.

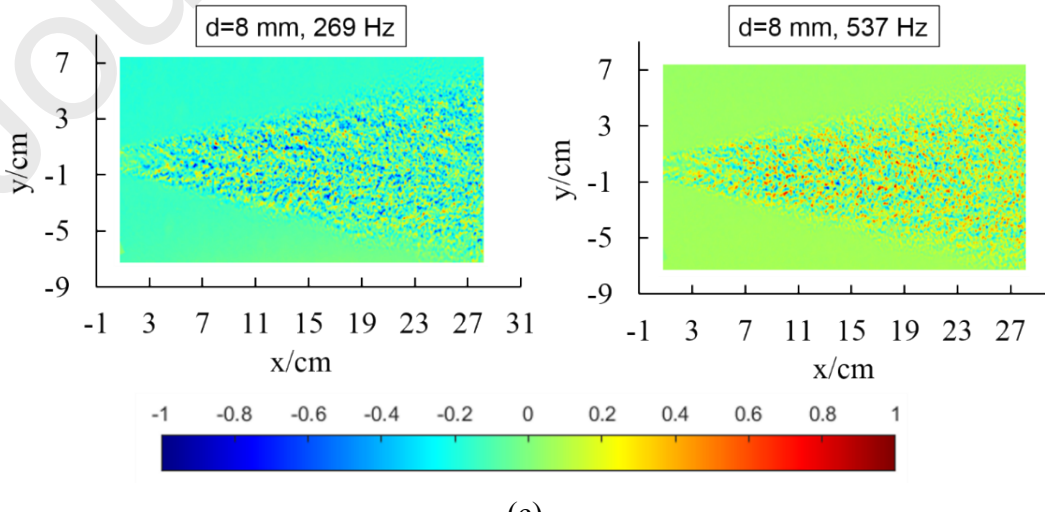

(c)

Fig.5 Spatial distribution of specific frequency modes (Test No.20).

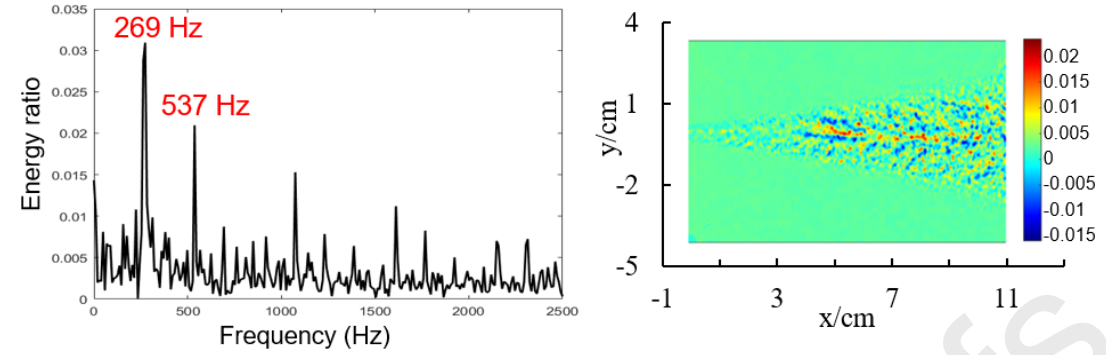

(a)

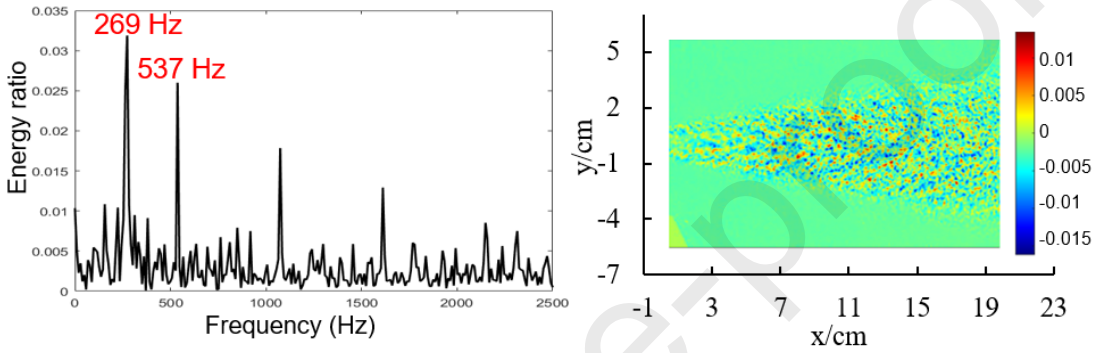

(b)

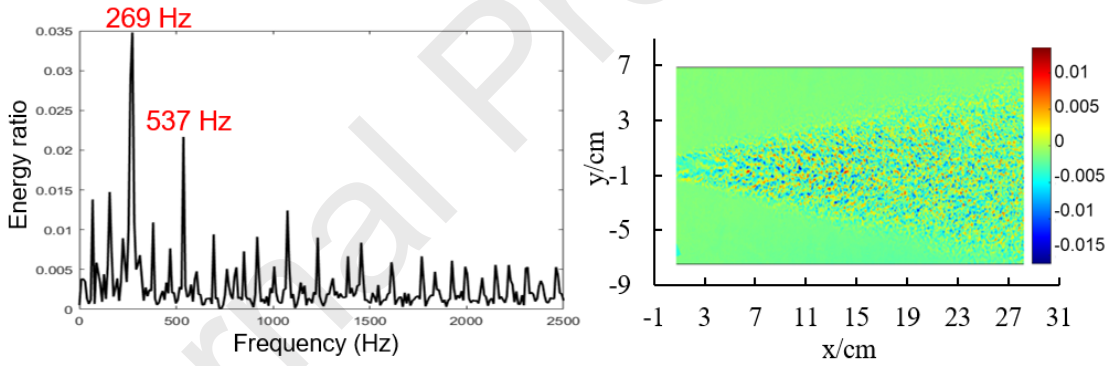

(c)

Fig.6 The spectral and spatial energy distribution of the first mode of POD analysis (a) Test No.2; (b) Test No.9; (c) Test No.20.

On the contrary, there is no obvious peaks appearing in the flame region, as shown in Fig.7. This may be due to the flame region is further downstream and less affected. The combustion heat release leads to significant increase in viscosity, which also tends to smooth out the high frequency. The DMD analysis has also been conducted on the whole color flame images (marked by the blue rectangle in Fig.3) as well as on the blue flame at the base region (marked by the red rectangle in Fig.3). The DMD analysis on flame images have shown a similar continuum distribution of the frequency spectra.

The peaks of 269 Hz can not be identified, since the imaging frequency (240 Hz) is too low.

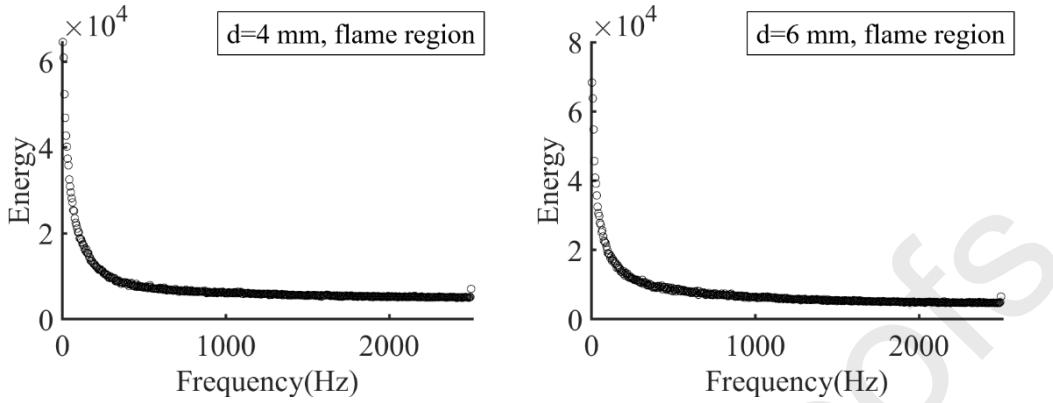

(a) (b)

Fig.7 Frequency spectra obtained from DMD analysis in flame region using schlieren images for (a) Test No.2, (b) Test No.9.

3.2 Flame structure parameter statistics

In the present study, three parameters were measured from flame images to represent the flame structure under different conditions, including horizontal flame length, flame height and lift-off distance. The flame images were firstly transferred to binary images using Otsu method [47]. The flame appearance probability contours were then obtained by adding up 100 binary images. Since the flame structure is fluctuating randomly due to turbulent characteristics, the appearance intermittency contour of 50% probability was employed to determine the flame geometric features. As shown in Fig.8, the horizontally and vertically projected flame length is measured as the distance from nozzle exit to the right and top edges of 50% appearance intermittency contour respectively. The horizontal distance between the 50% line at the flame base and the nozzle exit is measured as the lift-off distance. In the current experimental setup, the flames with the nozzle diameter at 8 mm are too long that the flame image is not able to show the whole structure. Thus the flame lengths and heights are measured and discussed only for test cases with nozzle diameters at 4 mm and 6 mm. The lift-off distances can be resolved for all the test cases listed in Table 2. The statistics of the aforementioned parameters are discussed in the following subsections.

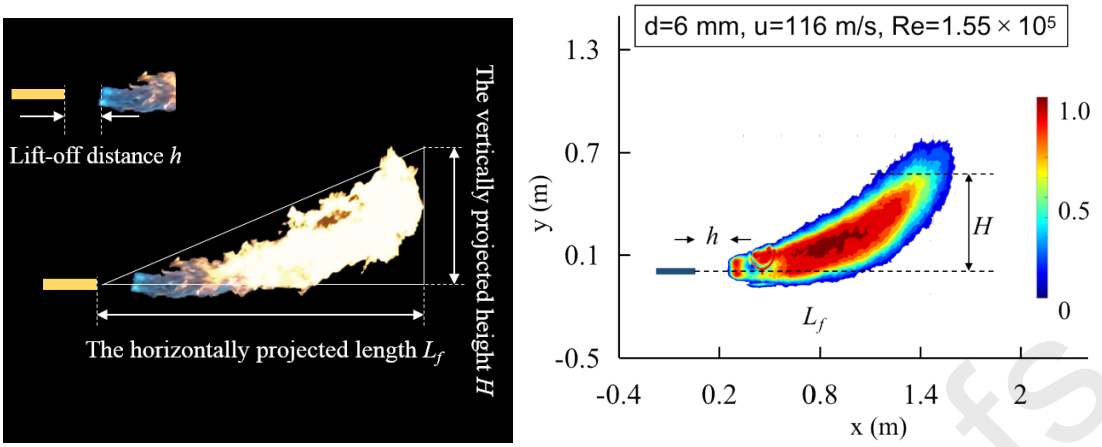

(a) (b)

Fig.8 (a) A sample flame image (Test No.9) and (b) the corresponding flame appearance probability contour

3.2.1 Horizontal flame length

The horizontal flame lengths measured in the current study have been presented in Fig.8, while similar data at lower speed conditions reported by Zhou et. al [38] are also presented for comparison. In Ref. [38], the propane jet flame is placed horizontally, while two round nozzles with sectional areas of 4 mm^2 (d=2.26 mm) and 16 mm^2 (d=4.51 mm) were adopted. The velocity is no more than 40 m/s. Four different plots have been used to represent the trend of horizontal flame length variations. For each figure, a fitting curve based on the measured data in Ref. [38] is presented. For convenience, the fitting curves in the corresponding data ranges are shown in our data figures. For the curve fitting in the present study, the coefficient of determination is evaluated by $R^2 = 1 - \frac{RSS}{TSS}$, where RSS is the sum of squares of residuals and TSS is the total sum of squares.

As shown in Fig.9(a), the flame length shows an increase trend with the nozzle exit velocity. It can be seen that when the flame is in the buoyancy-controlled region, as reported by Ref. [38], the flame length increases dramatically when the velocity starts to increase from a relatively small value. The increasing rate is decreasing with the increase of the velocity, which tends to a constant when the velocity increases to 30 m/s-40 m/s. The velocity range tested in Ref. [38] has involved the transition from

laminar to turbulent. The nonlinear trend indicates that with the increasing of nozzle exit velocity, momentum has a more significant effect on the flame length. For the test cases in current study, the linear trend has continued. The data sets of two nozzle diameters at 4 mm and 6 mm have collapsed to a single curve, which indicates the dominant role of momentum in this region.

Previous studies have shown that Froude number (*Fr*) is a key parameter for controlling jet flames. As shown in Table 2, almost all of the current test cases are in the momentum-controlled region ($Fr>1\times10^5$), while the data points reported in Ref. [38] were mainly in the buoyancy-controlled region ($Fr<1\times10^5$). A. L. Suris et al. [48] have proposed an equation that relates horizontal flame length and the Froude number, as

$$L_f / d = AFr^{0.2}, \tag{1}$$

where L_f is the flame horizontally length; d is the nozzle diameter; and the parameter A is related to fuel type, nozzle shape and diameter. As shown in Fig.9(b), the data sets in the present study are roughly follow a linear increasing trend, while some divergence can be observed for two nozzle diameters. The results for d=4 mm nozzle have shown a better coincidence with the linear fitting curve in Ref. [38]. Although the linear relationship exists in a wide range of flow conditions, the curves have shown deviations from each other. Meanwhile, the data of vertical flame length in Ref. [30] have been plotted for comparison, which also adopted Froude number as an independent variable. As can be seen from Fig.9(b), the length of horizontal flame shows roughly the same variation trend as the vertical flame, while the slope of vertical flame data is slightly lower than that of horizontal flame. The difference is mainly due to the buoyancy effect is more significant in the vertical flames.

The heat release rate is also adopted to relate with the non-dimensional horizontal flame length [49]. From their definition, the non-dimensional heat release rate Q^* is the square root of Froude number. Meanwhile, $(1-\chi_r)^{0.5}$ is used to consider the radiation effect, while χ_r = 0.3 is the radiative fraction [38]. As shown in Fig.9(c), it can be seen

that the data sets in the present study have collapsed to one linear line. For the data sets with lower velocities, a nonlinear trend was observed by Zhou et. al [38].

An equation has been proposed by Hu et. al [50] and Zhou et. al [38] to predict the horizontal flame length, which is listed below

$$L_f / d = \frac{(5\omega^2)^{3/5}(2\omega\zeta\kappa^2 + 25\omega^2 Q^{*2})^{1/5} - 2\omega\zeta}{5\omega^2}, \quad (2)$$

in which $\kappa = \frac{0.0059}{\pi/4}(\frac{\Delta h_c / \psi}{c_{p,\infty} T_\infty})^{1.5}(1-\chi_r)^{0.5}$, $\omega = 4C^2\kappa$, $\zeta = 4C\kappa$, and C is the phenomenological constant which is about 0.38 in circle nozzle. In the equation, Δh_c = 46,000 kJ/kg is the fuel combustion heat and ψ=15.6 is the air to fuel mass stoichiometric ratio. The air specific heat $c_{p,\infty}$ is 1.01 kJ/kg at $T_\infty = 298K$. The equation can predict the flame length well in a wide range of conditions regardless the fuel type, jet direction and nozzle shape. This equation has worked well for the data sets of Zhou et. al [38]. However, as shown in Fig.9(d), for the data sets in an extended velocity range in the current study, an obvious deviation can be observed. The data sets still collapse to a single line, which has a steeper slope than the one of Eq.2. The comparison also indicates that the flow conditions should be involved for flame length prediction.

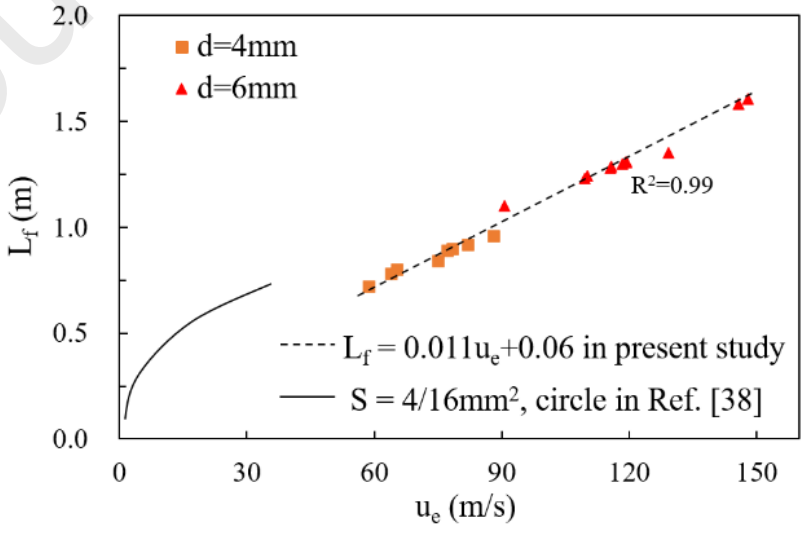

(a)

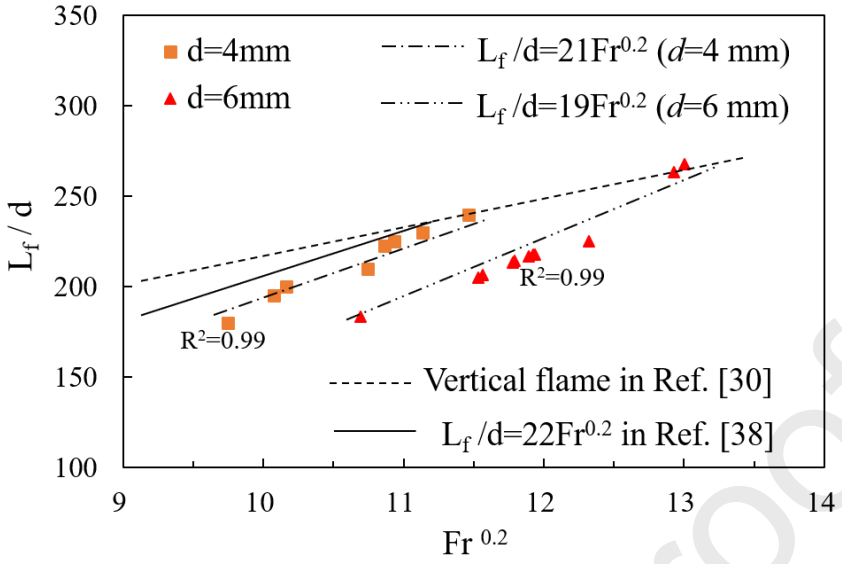

(b)

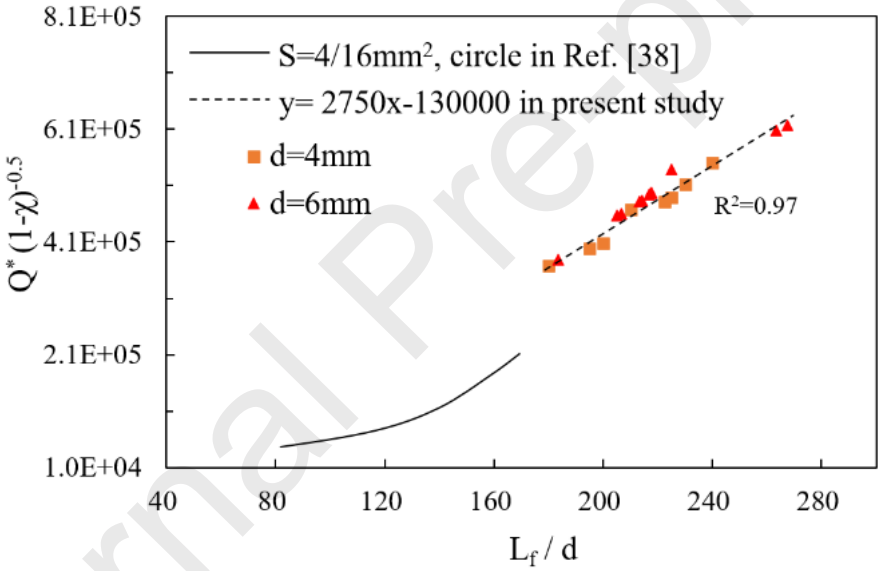

(c)

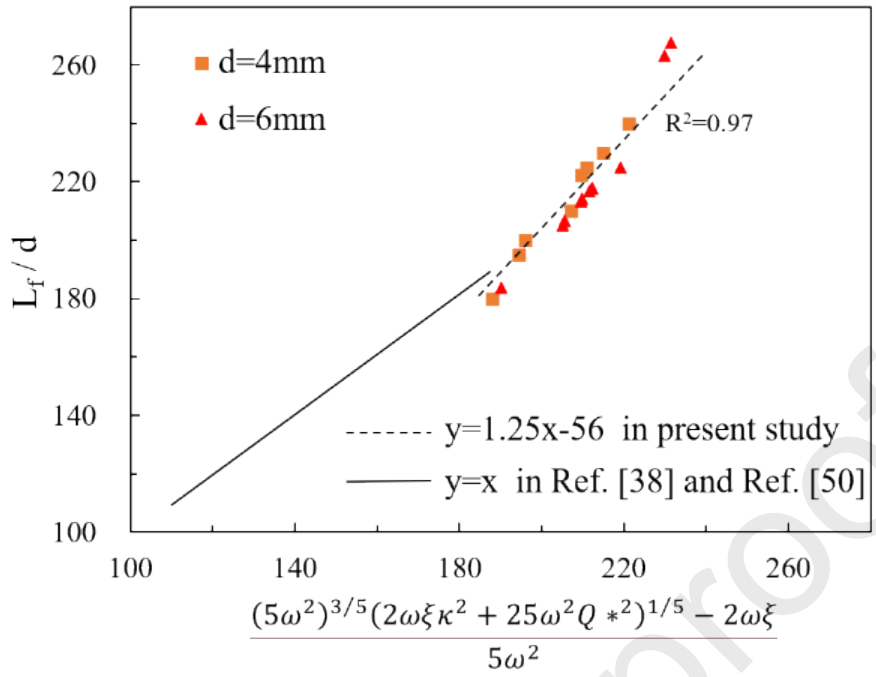

(d)

Fig.9 Plots of horizontal flame length

3.2.2 Flame height

For horizontal jet flames, the central line of the flame will go upward due to the buoyancy effect. The flame height versus jet exit velocity has been plotted in Fig.10(a), while the curve fit in Ref. [38] is also presented. It can be seen that the flame height is increasing with the jet velocity first and then a slightly decreasing trend can be observed for both data sets. The flame height reaches the maximum height at around 32 m/s in the buoyancy-controlled region, while the second maximum height appears around 138 m/s in the momentum-controlled region. If we look at the two data sets together in the whole velocity range, the flame height is decreasing during the transition from buoyancy to momentum-controlled region. This reflects the dual effects of buoyancy and momentum in horizontal jet flames. At low velocities, the buoyancy effect is more dominant. Thus the flame height is increasing along with the flame length at higher velocities. After a critical value, the momentum effect plays a more important role, which will suppress the flame height to a lower value. With the further increase of velocity, the flame height increases along with the whole flame being larger.

The horizontal flame shape can be quantitatively evaluated by the inclination angle

θ, which can be calculated by

$$\tan\theta = H / L_f . \quad (3)$$

In Eq.(3), H and L_f are the flame height and length respectively. The relative weight between buoyancy and moment effect can be depicted by Richardson number (Ri) [51], as:

$$Ri = \frac{\rho_\infty g H^3}{\rho_e S u_e^2} . \quad (4)$$

where ρ_∞ =1.29 kg/m^3 for ambient air; ρ_e is the fuel gas density at the exit; g is the acceleration of gravity; u_e is the exit velocity of the fuel and S is the nozzle exit area. When Ri is approaching infinitely large, the flame is totally vertical (θ=90 degree). If Ri is zero, then the flame will be horizontal (θ=0 degree). Zhou et. al [38] has related the inclination angle and Richardson number using the following equation,

$$H/L_f = 0.25(Ri)^{0.26} . \quad (5)$$

The data sets in the present study has also roughly collapsed to a single line as shown in Fig.10 (b), with a small deviation with Eq. (5), which is,

$$H/L_f = 0.27(Ri)^{0.26} . \quad (6)$$

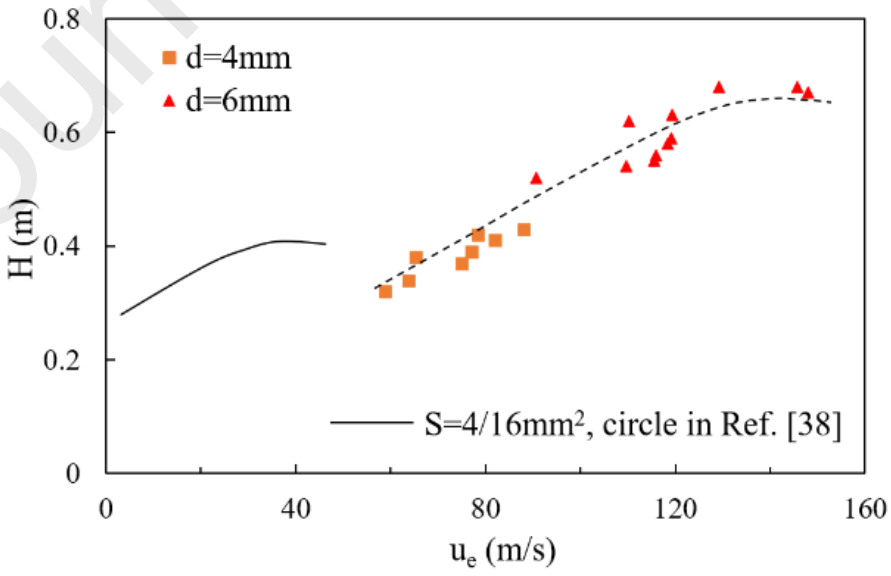

(a)

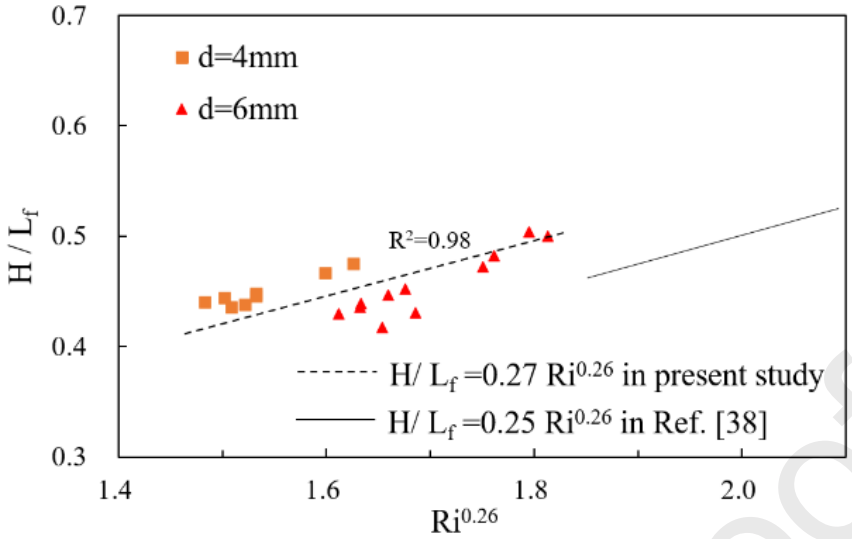

(b)

Fig.10 (a) Flame height at different velocities; (b) Relationship between flame inclination angle and Richardson number

3.2.3 Lift-off distance

The lift-off distance of the horizontal propane jet flame has been measured using the visible flame contour statistics. Previous experimental studies on propane vertical jet flame have shown that the lift-off distance varies linearly with the jet exit velocity and is independent of the burner diameter [11, 28, 52]. The lift-off distance measured in current investigation has also been plotted against the exit jet velocity, as shown in Fig.11(a). It can be seen that the lift-off height of horizontal jet flame in the test region also shows a roughly linear trend with the exit velocity, indicating weak relevance with the nozzle exit dimension. The fitting line is in good consistency with the further extension of the linear fitting reported in Ref. [38]. In previous studies, M.S. Cha et al. [28] studied the lifted flame characteristics of vertically non-premixed turbulent propane jets by experiments. Putting historical data fitting curve in the same figure, it can be seen that the lift-off distance of horizontal and vertical flame has shown very similar trend in a relatively wide range of velocities.

Recently, Bradly et al. [6] has proposed a dimensionless parameter U^* to fit the lift-off distance, which has shown a good linear trend for both vertical and horizontal jet flames. The definition of U^* is

$$U^* = (u_e / S_L)(S_L d / v_e)^{-0.4}, \quad (7)$$

where S_L is the maximum laminar burning velocity of fuel-air mixture; v_e is the fuel gas kinematic viscosity; and d is the nozzle diameter. The lift-off distance is also nondimensionalized as $H^* = h/d$, where h is the lift-off distance.

The linear fit by Zhou et. al [38] for the horizontal flame in the buoyancy region is

$$h/d = 3.02U^* - 5.38. \quad (8)$$

The data sets obtained in the present study have been plotted in Fig.11(b). It can be seen that the data collected for d=4 mm have shown good consistency with Eq.8 in the extended velocity region. The cases with d=6 mm and 8 mm have collapsed to another line, which has an obvious deviation from Eq.8. The fitting curve equation is

$$h/d = 1.9U^* - 8.2 \quad (d\text{=}6/8 \text{ mm}, u_e\text{=}90\text{-}167 \text{ m/s}) \quad (9)$$

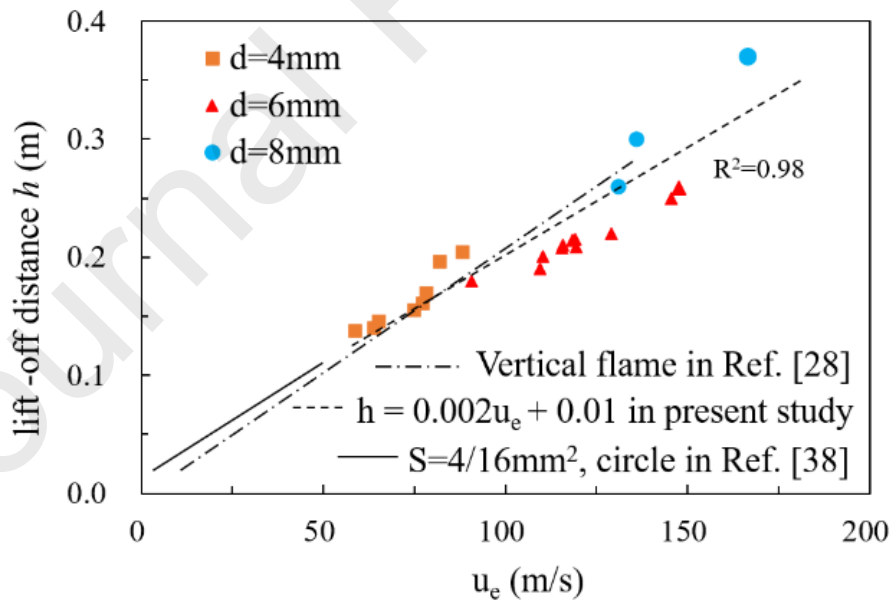

(a)

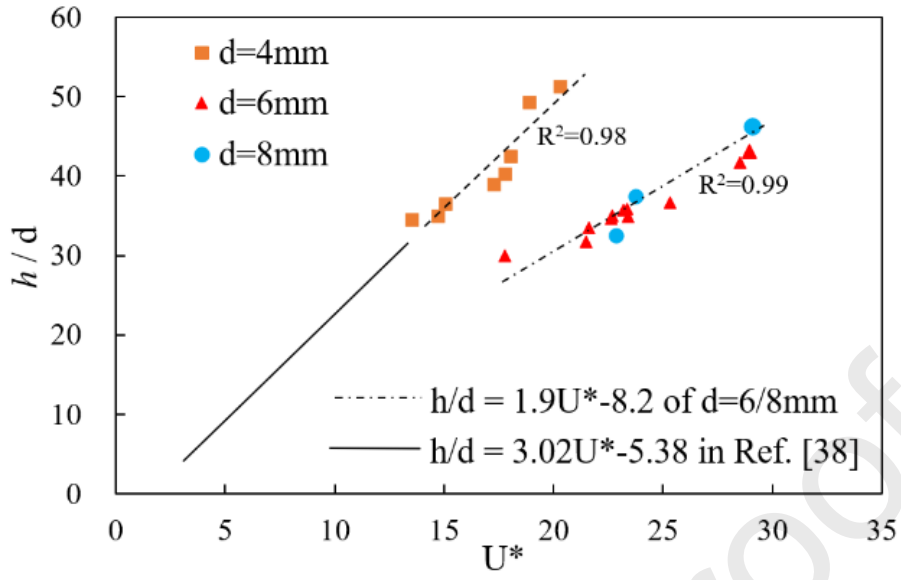

(b)

Fig.11 Variation of lift-off height with exit velocity

4 Conclusions

In this paper, horizontal lifted jet flames under relatively high velocity conditions have been investigated experimentally. Comprehensive analysis has been conducted to reveal the flame and flow dynamics, including frequency information, flame size and lift-off distance statistics. The DMD and POD analysis indicates that there are two distinct frequency signals in the lift-off jet region, which are independent of the nozzle diameter and Reynolds number. However, no obvious coherent structures can be observed on the spatial energy distribution. The frequency identified might come from the test bench vibration. The flame shape and lift-off distance statistics have been evaluated in both dimensional and dimensionless ways, while the low speed test data reported in the literature were also presented for comparison. Both flame length and height variations with velocity have shown deviations in low speed region (buoyancy-controlled) and high speed region (momentum-controlled), while some of the differences are quite dramatic. For the lift-off distance, the simple linear trend shows to be roughly correlated with the nozzle exit velocity, regardless of the nozzle diameter effect. However, two distinct linear lines have to be used to fit the data with different nozzle diameters in the plot with a specific dimensionless grouping. The results indicate

that the horizontal jet flame have shown dramatic differences in the buoyancy and momentum-controlled regions. Some of the scaling analysis has to be done separately at the present stage. The experimental data reported in this paper has enriched the data bank of horizontal jet flame in a wider velocity range, which are of great importance for deeper understanding of the complex flame and flow interactions.

Acknowledgements

This work has been partially done under Projects CTQ2017-85990-R funded by MCIN/ AEI /10.13039/501100011033/ FEDER "Una manera de hacer Europa" and PID2020-114766RB-100 funded by MCIN/ AEI /10.13039/501100011033. The research is also supported by the Leverhulme International Fellowship (ID/Ref: IAF-2019-034) to the Sheffield Group.

References

[1] Y.M. Annushkin, E.D. Sverdlov, Stability of submerged diffusion flames in subsonic and underexpanded supersonic gas-fuel streams, Combust. Expl. Shock Waves, 14(5) (1978) 597-605.

[2] W.M. Pitts, Assessment of theories for the behavior and blowout of lifted turbulent jet diffusion flames, Proc. Combust. Inst., 22(1) (1989) 809-816.

[3] B. Bra, C. Ap, Analysis of experimental blowout velocities of jet flames, Combust. Flame 213 (2020) 237-239.

[4] D.Y. Kiran, D.P. Mishra, Experimental studies of flame stability and emission characteristics of simple LPG jet diffusion flame, Fuel 86(10-11) (2007) 1545-1551.

[5] K.M. Lyons, Toward an understanding of the stabilization mechanisms of lifted turbulent jet flames: Experiments, Prog. Energy Combust. Sci. 33(2) (2007) 211-231.

[6] D. Bradley, P. H. Gaskell, X. Gu, A. Palacios, Jet flame heights, lift-off distances, and mean flame surface density for extensive ranges of fuels and flow rates, Combust. Flame 164 (2016) 400-409.

[7] S. Karami, E. Hawkes, M. Talei, J.Chen, Mechanisms of flame stabilisation at low lifted height in a turbulent lifted slot-jet flame, J. Fluid Mech. 777 (2015) 633-689.

[8] C.D. Brown, K.A. Watson, K.M. Lyons, Studies on lifted jet flames in coflow: the stabilization mechanism in the near- and far-fields, Flow Turbul. Combust. 62(3) (1999) 249-273.

[9] L. Muñiz, M.G. Mungal, Instantaneous flame-stabilization velocities in lifted-jet diffusion flames, Combust. Flame 111(1) (1997) 16-31.

[10] A. Joedicke, N. Peters, M. Mansour, The stabilization mechanism and structure of turbulent hydrocarbon lifted flames, Proc. Combust. Inst. 30(1) (2005) 901-909.

[11] G.T. Kalghatgi, Lift-off heights and visible lengths of vertical turbulent jet diffusion flames in still air, Combust. Sci. Technol. 41(1-2) (1984) 17-29.

[12] N.J. Moore, K.M. Lyons, Leading-edge flame fluctuations in lifted turbulent flames, Combust. Sci. Technol. 182(7) (2010) 777-793.

[13] A. Cessou, C. Maurey, D. Stepowski, Parametric and statistical investigation of the behavior of a lifted flame over a turbulent free-jet structure, Combust. Flame 137(4) (2004) 458-477.

[14] A. Upatnieks, J.F. Driscoll, C.C. Rasmussen, S.L. Ceccio, Liftoff of turbulent jet flames-assessment of edge flame and other concepts using cinema-PIV, Combust. Flame 138(3) (2004) 259-272.

[15] K.A. Watson, K.M. Lyons, J.M. Donbar, C.D. Carter, Simultaneous Rayleigh imaging and CH-PLIF measurements in a lifted jet diffusion flame, Combust. Flame 123(1) (2000) 252-265.

[16] T.F. Guiberti, W.R. Boyette, W.L. Roberts, A.R. Masri, Pressure effects and transition in the stabilization mechanism of turbulent lifted flames, Proc. Combust. Inst. 37(2) (2019) 2167-2174 .

[17] Q. Wang, L. Hu, M. Zhang, F. Tang, X. Zhang, S. Lu, Lift-off of jet diffusion flame in sub-atmospheric pressures: an experimental investigation and interpretation based on laminar flame speed, Combust. Flame 161(4) (2014) 1125-1130.

[18] S. Bang, B.J. Lee, S.H. Chung, Effect of pressure on the characteristics of lifted flames, Proc. Combust. Inst. 37(2) (2019) 2013-2020.

[19] K. Wohl, N.M. Kapp, G. Gazley, Flame Stabilization and propagation in high velocity gas stream, Proc. Combust. Inst.t 3 (1949) 3-21.

[20] S.R. Gollahalli, Ö. Savaş, R.F. Huang, J.L. Rodriquez Azara, Structure of attached and lifted gas jet flames in hysteresis region, Proc. Combust. Inst. 21(1) (1988) 1463-1471.

[21] D. Demare, F. Baillot, The role of secondary instabilities in the stabilization of a nonpremixed lifted jet flame, Phys. Fluids 13 (2001) 2662-2670.

[22] S. Hartl, R. Van Winkle, D. Geyer, A. Dreizler, G. Magnotti, C. Hasse, R.S. Barlow, Assessing the relative importance of flame regimes in Raman/Rayleigh line measurements of turbulent lifted flames, Proc. Combust. Inst. 37(2) (2019) 2297-2305.

[23] C.D. Brown, K.A.Watson, K.M. Lyons. Studies on Lifted Jet Flames in Coflow: The Stabilization Mechanism in the Near- and Far-Fields, FlowTurbul. Combust. 62

(1999)249-273.

[24] T.F. Guiberti, W.R. Boyette, Y. Krishna, W.L. Roberts, A.R. Masri, G. Magnotti. Assessment of the stabilization mechanisms of turbulent lifted jet flames at elevated pressure using combined 2-D diagnostics, Combust. Flame 214 (2020) 323-335.

[25] J.I. Erete, K.J. Hughes, L. Ma, M. Fairweather, M. Pourkashanian, A. Williams, Effect of CO2 dilution on the structure and emissions from turbulent, non-premixed methane-air jet flames, J. Energy Inst. 90(2) (2017) 191-200.

[26] L. Hu, Q. Wang, M. Delichatsios, F. Tang, X. Zhang, S. Lu, Flame height and lift-off of turbulent buoyant jet diffusion flames in a reduced pressure atmosphere, Fuel 109 (2013) 234-240.

[27] D.Y. Kiran, D.P. Mishra, Experimental studies of flame stability and emission characteristics of simple LPG jet diffusion flame, Fuel 86 (2007) 1545-1551.

[28] M.S. Cha, S.H. Chung, Characteristics of lifted flames in non-premixed turbulent confined jets, Proc. Combust. Inst. 26 (1996) 121–8.

[29] L. Hu, Q. Wang, M. Delichatsios, F. Tang, X. Zhang, S. Lu, Flame height and lift-off of turbulent buoyant jet diffusion flames in a reduced pressure atmosphere, Fuel 109 (2013) 234-240.

[30] N. Peters, J. Göttgens, Scaling of buoyant turbulent jet diffusion flames, Combust. Flame 85(1) (1991) 206-214.

[31] J.P. Gore, C.Q. Jian, Analytical solution to the flame trajectory based on the analysis of “Scaling of buoyant turbulent jet diffusion flames” by N. Peters and J. Göttgens, Combust. Flame 93(3) (1993) 336-337.

[32] B.J. Lowesmith, G. Hankinson, Large scale high pressure jet fires involving natural gas and natural gas/hydrogen mixtures, Process Saf. Environ. Protect. 90(2) (2012) 108-120.

[33] Q. Zhang, D. Liang, J. Wen, Experimental study of flashing LNG jet fires following horizontal releases, J. Loss Prev. Process Ind. 57 (2019) 245-253.

[34] H.A. Becker, D. Liang, Effect of burner orientation and ambient airflow on geometry of turbulent free diffusion flames, Proc. Combust. Inst. 18 (1981) 1061-1071.

[35] G. Heskestad, Turbulent jet diffusion flames: consolidation of flame height data, Combust. Flame 118(1-2) (1999) 51-60.

[36] G. Heskestad, Fire plumes, flame height, and air entrainment, SFPE handbook of fire protection engineering, Springer, New York, 2016.

[37] S. Liu, M.A. Delichatsios, L. Hu, Flame profile parameters of horizontal turbulent jets: Experiments, similarity analysis and an integral model, Combust. Flame 207 (2019) 1-9.

[38] K. Zhou, Y. Wang, L. Zhang, Y. Wu, X. Nie, J. Jiang, Effect of nozzle exit shape

on the geometrical features of horizontal turbulent jet flame, Fuel 260 (2020) 116356.

[39] T. Smith, C. Periasamy, B. Baird, S. Gollahalli, Trajectory and characteristics of buoyancy and momentum dominated horizontal jet flames from circular and elliptic burners, J. Energy Resour. Technol. 128 (2006) 300-310.

[40] V. Foroughi, A. Palacios, C. Barraza, A. Àgueda, C. Mata, E. Pastor, J. Casal, Thermal effects of a sonic jet fire impingement on a pipe, J. Loss Prev. Process Ind. 71(4-6) (2021) 104449.

[41] P.J. Schmid, L. Li, M.P. Juniper, O. Pust, Applications of the dynamic mode decomposition, Theor. Comp. Fluid Dyn. 25(1-4) (2011) 249-259.

[42] P.J. Schmid, J. Sesterhenn, Dynamic mode decomposition of numerical and experimental data, J. Fluid Mech. 656(10) (2010) 5-28.

[43] G. Matthew, M.G. Berry, Y. Mohd, M.N. Glauser, DMD and POD of time-resolved schlieren on a multi-stream single expansion ramp nozzle, Int. J. Heat Fluid Flow 67 (2017) 42-51.

[44] J. Peng, G. Long, Y. Xin, F. Qin, B. Liu, Z. Cao, G. Wu, M. Han. Combustion oscillation characteristics of a supersonic ethylene jet flame using high-speed planar laser-induced fluorescence and dynamic mode decomposition, Energy. 239 (2022) 122330.

[45] Q. Wang, J.T. Wang, X.H. Mei, Y.C. Sun, M.B. Sun, J.J. Zhu, C.Y. Zhao, Imaging-based harmonic frequency analysis of a bluff-body premixed flame under acoustic excitations, Aerosp. Sci. Technol. 120 (2022) 107254.

[46] J.N. Kutz, X. Fu, S.L. Brunton, Multi-resolution dynamic mode decomposition, SIAM J. Appl. Dyn. Syst. 15 (2) (2016) 713–735.

[47] N. Otsu, A Threshold selection method from gray-level histograms, IEEE Trans. Syst. Man Cyber 9(1) (1979) 62-6.

[48] A.L. Suris, E.V. Flankin, S.N. Shorin, Length of free diffusion flames, Combust. Expl. Shock Waves. 13(4) (1977) 459-462.

[49] S.A. Reodikar, H.C. Meena, R. Vinze, S.V. Prabhu, Influence of the orifice shape on the local heat transfer distribution and axis switching by compressible jets impinging on flat surface, Int. J. Therm. Sci. 104 (2016) 208-224.

[50] L. Hu, X. Zhang, X. Zhang, L. Yang, A re-examination of entrainment constant and an explicit model for flame heights of rectangular jet fires, Combust. Flame 161(11) (2014) 3000-3002.

[51] H.A. Becker, D. Liang, C.I. Downey, Effect of burner orientation and ambient airflow on geometry of turbulent free diffusion flames,Proc. Combust. Inst. 18(1) (1981) 1061-1071.

[52] N.A. Røkke, J.E. Hustad, O.K. Sønju, A study of partially premixed unconfined

propane flames, Combust. Flame 97 (1994) 88-106.

Highlights

1. Horizontal flame jets in momentum-controlled region are studied experimentally.
2. The lift-off distance, flame length and height statistics are measured and discussed.
3. The observed flame characteristics is quite different with low velocity conditions.
4. The high velocity conditions have enriched the horizontal jet flame data bank.

Declaration of interests

☒ The authors declare that they have no known competing financial interests or personal relationships that could have appeared to influence the work reported in this paper.

☐ The authors declare the following financial interests/personal relationships which may be considered as potential competing interests:

Author statement

Q. Wang (First Author, Corresponding Author): Conceptualization, Methodology, Investigation, Formal Analysis, Writing - Original Draft; Writing - Review & Editing.

P. Zhu: Data Curation, Visualization, Writing - Original Draft.

X.H. Mei: Data Curation, Visualization.

V. Foroughi: Data Curation.

J. Casal: Data Curation.

E. Planas: Conceptualization, Funding Acquisition, Resources, Supervision, Writing - Review & Editing.

A. Albadi: Data Curation.

Y.C. Zhang: Data Curation.

Y. Zhang (Corresponding Author): Conceptualization, Funding Acquisition, Resources, Supervision, Writing - Review & Editing.